Modeling Power Semiconductor Losses in HEV Powertrains using Si and SiC Devices

Justin K. Reed[1], James McFarland[1], Jagadeesh Tangudu[1], Emmanuel Vinot[2], Rochdi Trigui[2], Giri Venkataramanan[1], Shiv Gupta[1], Thomas Jahns[1]

[1]Dept. of Electrical and Computer Engineering
University of Wisconsin-Madison
Madison, WI 53706, USA
Email: jkreed@ieee.org

[2]INRETS (The French National Institute for Transport and Safety Research), Transport and Environment Laboratory
25 Ave François Mitterand – 69675 Bron Cedex, France

***Abstract*- Silicon carbide (SiC) power semiconductor devices are known to have potential benefits over conventional silicon (Si) devices, particularly in high power applications such as hybrid electric vehicles (HEVs). Recent literature studying the use of SiC JFETs in HEV inverters indicate a substantially increased gas mileage. This paper further investigates this change in inverter efficiency due to the adoption of SiC using analytical loss models and empirical loss data obtained from experimental Cree 1200V 10A DMOSFETs and Schottky diodes. A motor inverter efficiency map is developed and used in the VEHLIB simulator to evaluate fuel consumption benefits. Distribution of conduction and switching losses in both Si and SiC inverters is explored.**

***Keywords*-Silicon carbide; ac-dc power conversion; power electronics; propulsion.**

I. INTRODUCTION

Power electronic converters form a critical technology in the emerging future automotive systems incorporating electric traction to supplement conventional mechanical traction elements utilizing internal combustion engines. In these systems, the electromechanical systems that enable the combustion engine to operate in their optimal operating regime are controlled using power electronic converters to manage energy flow among the wheel demand, combustion engine and storage device. The operating envelope and self-heating in the power converters themselves play an important role in determining system controllability, reliability and potentially affecting overall fuel efficiency. This paper is aimed at developing and presenting a loss model for determining losses in the power converter during candidate drive cycles. Furthermore, recent studies indicate a large potential for performance improvement while utilizing SiC devices either in place of Si devices or augmenting Si devices in the power converters. The model developed herein may be used to evaluate the performance metrics conveniently on the basis of behavioral models and test data on the devices.

In particular, silicon carbide (SiC) MOSFETs are an emerging technology that has the potential to offer improved performance over conventional silicon (Si) MOSFETs in power converters. The SiC material itself has much lower thermal resistance and can withstand higher junction temperatures. Electrical performance is also improved with higher blocking voltages and faster switching speeds. Some applications of SiC, which take advantage of these properties have been investigated [1,2], including in hybrid-electric vehicles (HEVs) [3].

One particular study based on PSAT simulations [4] indicated a potential improvement of 18.3% in gas mileage by direct replacement of Si IGBTs with SiC JFETs of expected future characteristics in the drivetrain inverters (SiC Schottky diodes were used in both cases), however physical implications and generalized reasoning for this behavior remain unclear. This paper further investigates the impact of SiC power semiconductors on vehicle performance using a 2004 Toyota Prius and empirical loss data for SiC MOSFETs extrapolated from experimental Cree 1200V 10A DMOSFETs. Conduction and switching losses are quantified, compared, and integrated into motor inverter efficiency maps. Fuel consumption benefits are quantified using the VEHLIB simulator [5].

II. EFFICIENCY MODELING APPROACH

One approach to evaluating drivetrain efficiency is to use inverter efficiency maps covering the torque-speed range of the 50 kW motor as illustrated in Fig. 1. This approach permits the system designers to optimize system efficiency by identifying and avoiding any regions of poor efficiency during typical drive cycles. The 2004 Prius inverter efficiency map in Fig. 2 indicates very high efficiency (>98%) above 2300 RPM and efficiency as low as 86% below 2300 RPM [6]. Therefore, significant gains in gas mileage would most likely result from efficiency improvements in the low speed range. This hypothesis is

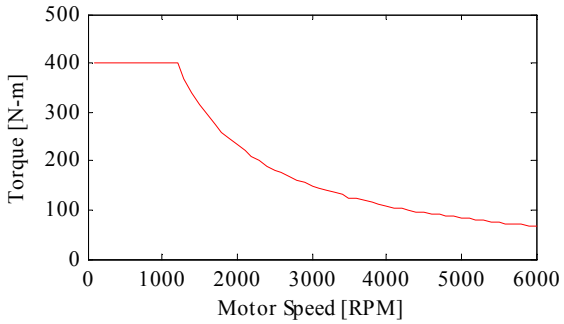

Fig. 1. Approximate 2004 Prius 50kW motor torque-speed envelope.

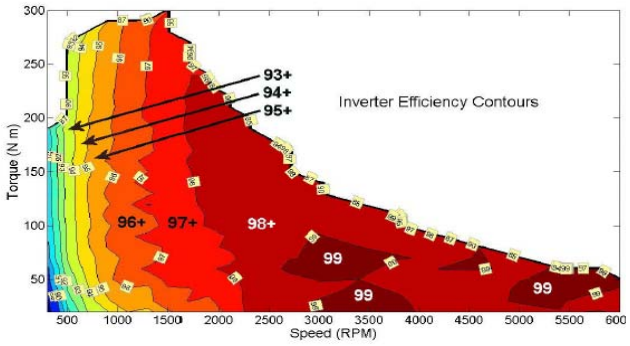

Fig. 2. 2004 Prius inverter measured efficiency map over torque-speed range of motor (reproduced from [6]).

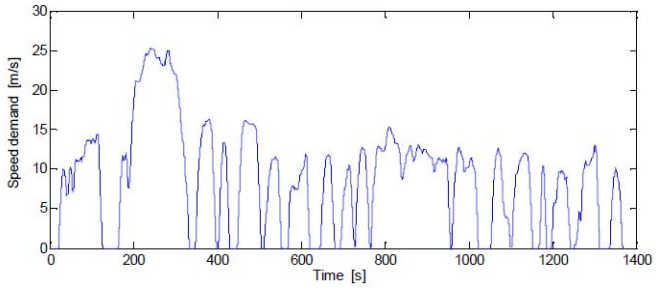

Fig. 3. A graph of UDDS drive cycle used in [4].

alluded to in [4], to utilize the US EPA Urban Dynamometer Driving Schedule (UDDS) in Fig. 3 to determine semiconductor losses and largely comprises low speed, stop-and-go driving.

The overall loss modeling process is depicted in Fig. 4. Operating points covering the torque-speed range of the motor are converted into voltage, current, and power factor angle operating points using a motor model developed using Finite Element Analysis (FEA) of the motor geometric design. These motor operating variables define the electrical operating conditions for the inverter, and in turn used in the inverter loss model to calculate losses with Si- and SiC-based inverters. Finally, the inverter efficiency plots are generated over the range of motor torque-speed plane. This data may be used with a vehicle model to obtain drive cycle efficiencies.

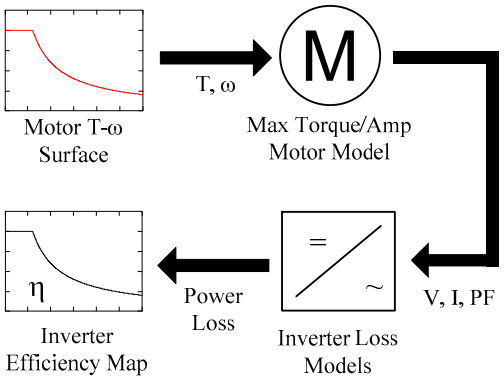

Fig. 4. Inverter loss and efficiency modeling process

III. Electric Machine Modeling

A motor model was developed to translate the torque-speed coordinates of Fig. 1 into terminal voltages and currents at the 50 kW motor terminals. This was accomplished using the JMAG FEA simulation package [7], in which a 2004 Prius motor was modeled as a 2D lossless machine based on known physical and electrical data [6,8,9]. FEA simulations were performed at different operating phase RMS currents $|I_{rms}|$ and internal/torque angles γ and their corresponding phase flux linkages are captured at each operating point.

While obtaining *d*- and *q*- axis flux linkages, each of these flux linkages are spatially averaged in the following manner. The rotor is rotated over 1/6th of an electrical cycle in steps of 1/72nd of an electrical cycle at each operating point (I_{rms} and γ). The corresponding phase flux linkages are computed and converted into the rotating reference frame at each rotation step. These instantaneous values of *d*- and *q*- axis flux linkages are then averaged over 1/6th of an electrical cycle to provide the recorded values. This technique makes it convenient to capture the spatial fundamental components of the *d*- and *q*-axis flux linkages [10].

The *d*- and *q*- axis flux linkages obtained in this manner essentially define the characteristics of a given machine and these flux linkages are then used in a custom built program to estimate the operating points based on maximum torque per ampere (MTPA) trajectory using MATLAB [11]. The resulting *d*- and *q*-axis stator fluxes at each MTPA operating point produce torque values according to

$$T(I_{rms},\gamma) = \frac{3}{2}\frac{p}{2}\left[\psi_d(I_{rms},\gamma)\cdot I_{rms}\cdot\cos(\gamma) - \psi_q(I_{rms},\gamma)\cdot I_{rms}\cdot\sin(\gamma)\right] \quad (1)$$

where p=8 poles. Using the FEA results that correspond to a particular MTPA operating condition, corresponding machine stator voltage V_s, stator current I_s and power factor (PF) were calculated. This process was repeated over the entire torque-speed envelope of the motor to obtain the terminal excitation values required to obtain MTPA for all conditions. A resulting plot of PF across the torque speed envelope is shown in Fig. 5.

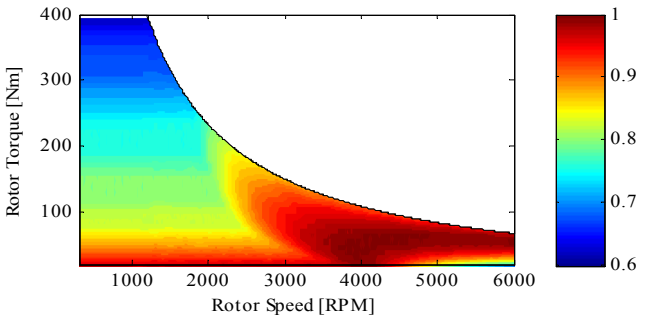

Fig. 5. A graph of 2004 Prius 50 kW motor power factor corresponding to MTPA over its operating range

IV. Si Inverter Loss Modeling

Inverter losses were calculated at each operating point based on the terminal voltage, current, and PF dictated by the motor model, assuming a constant 500V dc bus. Total Si losses were represented as the sum of IGBT and diode conduction and switching losses,

$$P_{Si\_loss} = P_{Si\_IGBT\_c} + P_{Si\_di\_c} + P_{Si\_sw}, \tag{2}$$

where the conduction losses of the Si IGBTs were determined using a first-order dynamic resistance model based on the high-frequency averaged device current I_{av} and collector-emitter voltage V_{ce}, and then averaged over one fundamental low-frequency ac cycle,

$$\begin{aligned} P_{Si\_IGBT\_c} &= \frac{1}{T}\int_0^T I_{av}\cdot V_{ce}(I_{av})dt \\ &= \frac{1}{T}\int_0^T I_{av}\cdot\left[V_{ce\_cut} + R_{ce}I_{av}\right]dt. \end{aligned} \tag{3}$$

The diode conduction losses are modeled using a similar dynamic resistance model,

$$\begin{aligned} P_{Si\_di\_c} &= \frac{1}{T}\int_0^T I_{av}\cdot V_{Si\_f}(I_{av})dt \\ &= \frac{1}{T}\int_0^T I_{av}\cdot\left[V_{Si\_f\_cut} + R_{Si\_f}I_{av}\right]dt, \end{aligned} \tag{4}$$

where V_{Si_f} is the Si diode forward voltage.

The 2004 Prius motor inverter uses 2 each of 850V 200A IGBT and diode dies in parallel [12] per switch. Loss parameters were estimated based on similar devices of the same generation, the 600V 200A IXYS IXGN 200N60B IGBT and 600V 300A IXYS MEA300-06 FRED, which are shown in Table I. Due to the lack of published loss data on the Prius devices, the switching losses were modeled by subtracting the modeled semiconductor conduction losses from the total measured inverter losses [6], curve fitting the difference (as a function of motor rms phase current I_{rms}) to the form [13]

$$P_{diff} = a_{Si\_1} + a_{Si\_2}\sqrt{I_{rms}} + a_{Si\_3}I_{rms} + a_{Si\_4}I_{rms}^{\ 2} \tag{5}$$

and setting $a_{Si\_4} = 0$,

$$P_{Si\_sw} = a_{Si\_1} + a_{Si\_2}\sqrt{I_{rms}} + a_{Si\_3}I_{rms}. \tag{6}$$

A limitation of this method is that it cannot completely isolate switching and conduction losses due to the a_{Si_3} term. However, the switching losses are dominated by a_{Si_2} due to the Si diode reverse recovery effect, hence a_{Si_3}'s contribution is small and the utility of the method is not compromised. The loss model neglects secondary loss contributors, e.g. capacitor ripple current, interconnect losses and housekeeping power. Junction temperature is assumed to be $T_j = 90°C$.

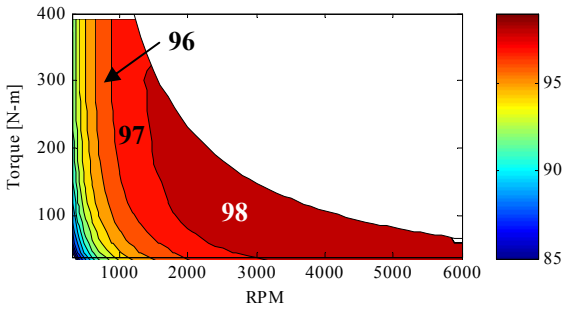

Fig. 6. A graph of Si inverter efficiency map providing model validation.

Fig. 6 shows a reproduction of Fig. 2 using the Si inverter model over the entire motor operating range. The degree of correlation between Fig. 6 and Fig. 2 may be readily observed.

V. SiC Inverter Loss Modeling

Although different loss mechanisms and the availability of physical devices require the use of a different modeling technique for the SiC components, their losses were similarly represented as the sum of conduction and switching losses of both the MOSFETs and diodes,

$$P_{SiC\_loss} = P_{SiC\_MOSFET\_c} + P_{SiC\_di\_c} + P_{SiC\_sw}. \tag{7}$$

The candidate SiC components used in this paper are based on 1200V 10A DMOSFETs manufactured by Cree and packaged in a 6-pack SEMIKRON SEMITOP package, shown in Fig. 7. Since the total rating of the actual Prius motor inverter components is 850V 400A, for an equivalent SiC rating, the model predictions are based on $N_{FET} = 40$ MOSFETs connected in parallel. MOSFET conduction losses were calculated using

$$P_{SiC\_MOSFET\_c} = I_{rms}^{\ 2}R_{ds\_on}, \tag{8}$$

where $R_{ds\_on} = 0.149\Omega$ per 10A MOSFET at room temperature (20 °C), or 3.71mΩ per Prius-rated device.

The SiC diode conduction losses are calculated with (4) using parameters $V_{SiC\_f\_cut}$ and R_{SiC_f}. The loss parameters shown in Table I represent both the paralleled Prius-rated devices and the individual 10A devices in parentheses. SiC switching losses were represented as

$$P_{SiC\_sw} = \frac{3N_{FET}F_s}{T}\int_0^T\left[E_{on}\left(\frac{|I_s|}{N_{FET}}\right) + E_{off}\left(\frac{|I_s|}{N_{FET}}\right)\right]dt. \tag{9}$$

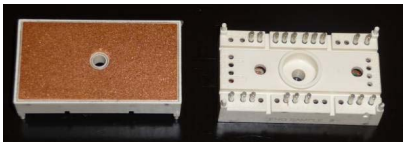

Fig. 7. Experimental Cree 1200V 10A SiC DMOSFET 6-pack within a SEMIKRON SEMITOP package.

Calculation of total SiC switching energy at 500V dc bus was performed using the averaging method of [13] with varying dc currents. Due to the high voltage and physical limitations of producing duty ratios small enough to output rated current with a short-circuited output, a 25Ω resistor was added to the 5.8mH output inductor. Gate resistance $\underline{R_g}$ = 30Ω for minimizing excitation of parasitic resonances. Maximum gate voltage V_{gs} = 14V. Losses were measured at switching frequencies F_s = 15kHz, 20kHz, 25kHz, and 30kHz. Measurements were performed with a Newtons4th PPA2630 power analyzer by integrating and averaging over 1-minute intervals for all data points.

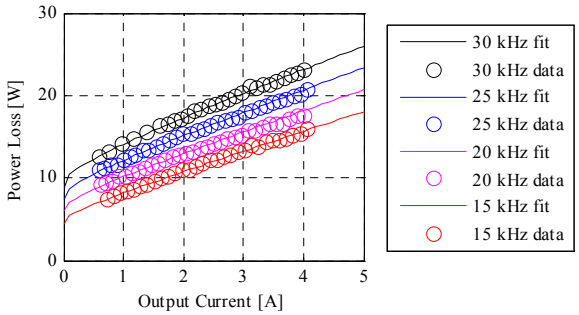

Fig. 8. Curve fitting of loss data with zero I^2 component.

It is known that SiC diodes exhibit far less reverse recovery effect than even ultrafast Si diodes. Therefore a satisfactory curve fitting of the converter power throughput was achieved by modifying the fitting to the form

$$P_{loss} = a_{SiC\_1} + a_{SiC\_2}\sqrt[3]{I_{dc}} + a_{SiC\_3} I_{dc} + a_{SiC\_4} I_{dc}^{\,2}. \qquad (9)$$

Fig. 8 shows the curve fit after setting $a_{SiC\_4} = 0$. Normalizing the differences in losses to the Prius inverter's 5kHz switching frequency [14] and calculating

$$E_{on}\left(\frac{|I_s|}{N_{FET}}\right) + E_{off}\left(\frac{|I_s|}{N_{FET}}\right) = \frac{P_{loss}\left(|I_s|/N_{FET}\right)}{5kHz} \qquad (10)$$

results in the switching energy (E_{on} + E_{off}) shown in Fig. 9.

TABLE I
DEVICE LOSS PARAMETERS

Parameter	Description	Value	Units
V_{ce_cut}	Si IGBT cut-in voltage	1.4	V
R_{ce}	Si IGBT dynamic resistance	5.8	mΩ
$V_{Si\_f\_cut}$	Si diode cut-in voltage	1.1	V
R_{si_f}	Si diode dynamic resistance	1.1	mΩ
$V_{SiC\_f\_cut}$	SiC diode cut-in voltage	0.89	V
R_{SiC_f}	SiC diode dynamic resistance	1.63 (65.2)	mΩ
R_{ds_on}	SiC MOSFET on-resistance	3.71 (149)	mΩ
a_{Si_1}	Si switching loss coefficient	25	W
a_{Si_2}	Si switching loss coefficient	27	$W \cdot A^{-1/2}$
a_{Si_3}	Si switching loss coefficient	0.074	V
a_{SiC_1}	SiC switching loss coefficient	57 (1.4)	W
a_{SiC_2}	SiC switching loss coefficient	18 (0.45)	$W \cdot A^{-1/3}$
a_{SiC_3}	SiC switching loss coefficient	3.3 (0.083)	V

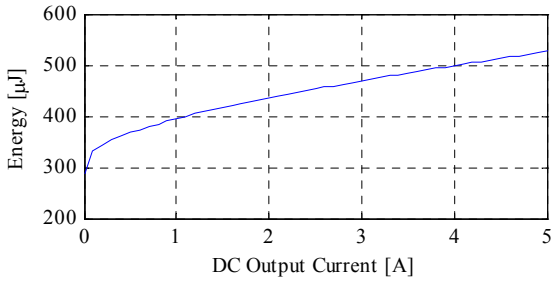

Fig. 9. Total SiC switching energy (E_{on} + E_{off}) of a 10A device at 500V.

VI. Comparison of Si and SiC Devices in 2004 Prius

A thorough comparison of Si and SiC devices is made based on conduction losses, switching losses, overall efficiency and fuel consumption.

A. Conduction Losses

While IGBTs are generally known to exhibit less conduction losses at high currents than MOSFETs due to the MOSFET's I^2R loss mechanism, the SiC MOSFET breaks this trend, showing outstanding conduction loss characteristics. Conduction loss plots are shown in Fig. 10.

B. Switching Losses

IGBTs are known to have significant switching losses, largely due to their tail currents, thus MOSFETs are often expected to have superior switching loss characteristics. SiC MOSFETs, however, also have relatively significant switching losses particularly at low currents, as has been documented in recent literature [2]. Notable aspects in the quantification of SiC switching losses developed here include the use of higher R_g to reduce parasitic ringing, consideration of secondary/parasitic losses, higher dc voltage, different V_{gs}, averaged measurements instead of instantaneous measurements, and of course different prototype devices. Despite these differences, our work confirms the significance of switching losses, shown in Fig. 11. It can be seen that Si has lower switching losses at low currents/torques, while SiC has lower switching losses at high currents/torques. It is therefore important to consider the total losses for both types of semiconductors to issue a valid comparison.

In this study, the dc bus voltage was fixed at 500V for both simplicity and to permit the use of loss data from [6]. However, since the actual dc bus varies between 200V and 500V, this work represents a worst-case scenario in that the switching losses also vary in a more complex manner than could be modeled in this study.

C. Overall Efficiency

The efficiency of the SiC inverter considering both conduction and switching losses is shown in Fig. 12, which can be compared to the Si inverter efficiency in Fig. 6. To assist in the comparison, Fig. 13 shows the loss reduction using an SiC inverter over an Si inverter, with a dotted red line to indicate where the losses are equal (SiC inverter has greater efficiency above the red line).

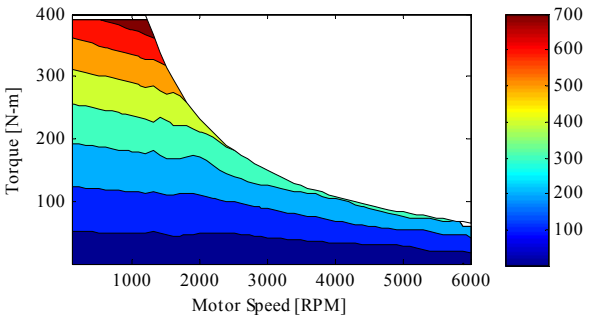

(a) Si IGBTs

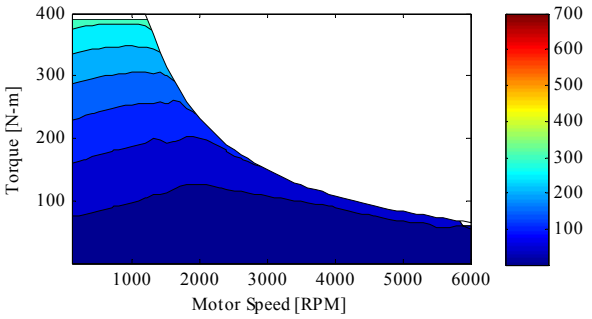

(b) SiC MOSFETs

Fig. 10. A surface plot of inverter semiconductor conduction losses across the torque speed envelope [W].

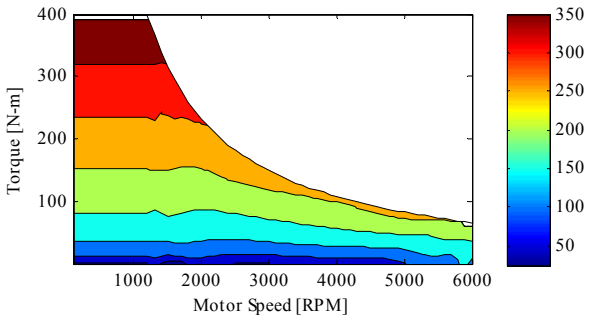

(a) Si IGBTs

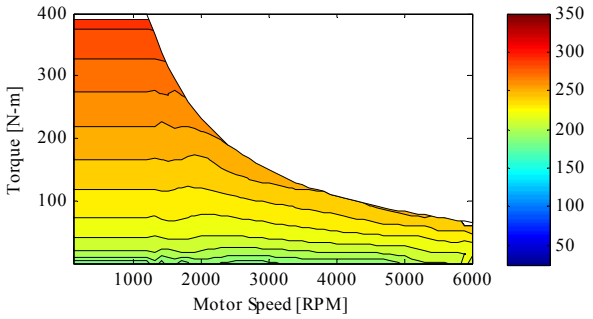

(b) SiC MOSFETs

Fig. 11. A surface plot of inverter semiconductor switching losses across the torque speed envelope [W]

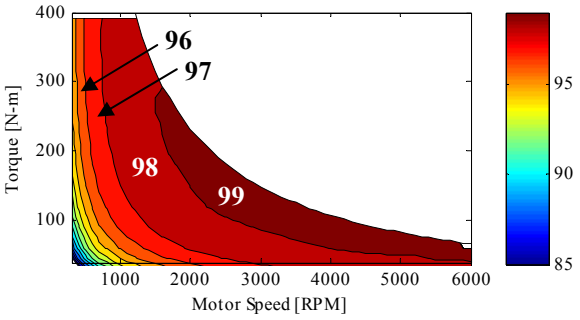

Fig. 12. A surface plot of SiC inverter efficiency map across the torque speed envelope [W]

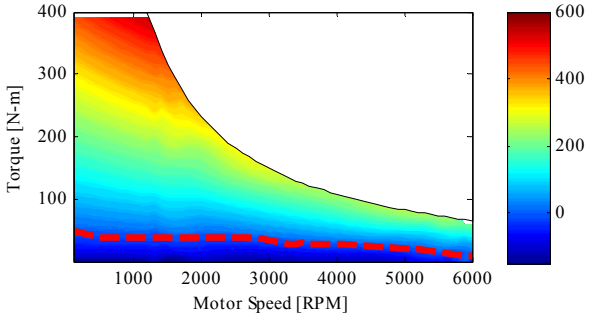

Fig. 13. A surface plot of loss reduction using an SiC inverter over an Si inverter across the torque speed envelope [W], with a red line that indicating the contour of equal losses.

D. Fuel Consumption

Efficiency maps of the Si and SiC inverters were applied to a 2004 Prius model in the VEHLIB hybrid vehicle simulator. Fuel consumption and motor + inverter losses were calculated over a US EPA UDDS drive cycle, as well as the European Urban, Road, and Motorway Artémis drive cycles. In an effort to reduce total semiconductor losses, a second SiC inverter was also simulated using only 30 MOSFETs per switch, thus achieving reduced switching losses at the expense of slightly increased conduction losses while remaining within the current ratings of the individual devices.

Numerical results for all 3 cases are shown in Table II. Fuel consumption of both SiC inverters is also expressed as a percentage change compared to baseline Si fuel consumption, shown in Fig. 14. These findings show that the maximum benefit seen by adopting SiC is a 1.85% reduction in fuel consumption, which occurs in the Urban Artémis drive cycle using 30 SiC MOSFETs per switch. Using the full 40 devices reduces this benefit to 0.69%. In all other drive cycles, the 40 device SiC inverter performed slightly worse than the stock Si inverter.

Based on these results, it is evident that adopting SiC MOSFETs in an HEV inverter can have either a slightly positive or slightly negative effect on overall vehicle fuel consumption depending on how the vehicle is used (i.e. which regions of the torque speed surface are used most frequently) and how many SiC devices are used to realize the inverter switches.

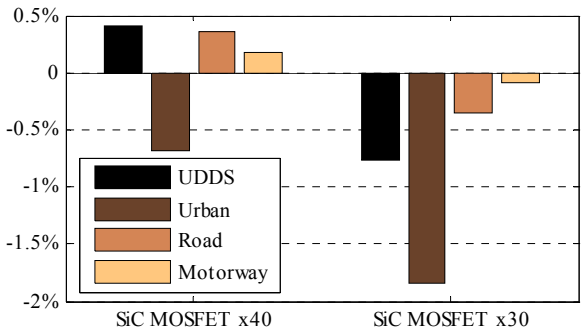

Fig. 14. Percent change in fuel consumption for different numbers of SiC MOSFETs in parallel per switch over various drive cycles, using Si inverter as baseline.

VII. Conclusions and Future Work

The application potential of SiC has been investigated for use in a 2004 Prius, based on experimental Cree SiC 1200V 10A MOSFETs with Schottky diodes. These devices were compared to the vehicle's stock dual 850V 200A Si IGBTs and diodes, using simple conduction and switching loss models in conjunction with an FEA-based motor model to provide appropriate terminal voltage, current and PF values over its operating space.

SiC conduction losses were found to be far less than those of the Si IGBTs, while the switching losses gave a less straightforward comparison. At low currents the SiC switching loss can be greater than the Si switching loss, while the opposite is true at high currents, which ultimately can impact the overall inverter efficiency depending on the relative weighting of conduction and switching losses. This presents the opportunity to optimize the SiC inverter design with regards to how many MOSFETs to connect in parallel to achieve a satisfactory balance of switching and conduction loss.

Fuel consumption was calculated using the VEHLIB simulator over 4 drive cycles and 3 inverter configurations. Overall changes in fuel consumption as compared to the Si baseline were minimal and even fared slightly worse in most cases when using SiC devices to realize switches of equal current rating to the stock Si baseline. A slight improvement of fuel consumption was seen by reducing the current rating of the switch from 400A to 300A, which effectively reduces switching losses while increasing conduction losses, albeit at a net reduction of the total loss.

Continuing work in refining the modeling approach would account for reduced switching losses with a variable dc bus voltage and would yield more accurate results, especially at low torques where overall inverter losses are largely dominated by the switching losses. The work here has not considered the effect of higher temperature operation of the power pack and/or the advantages that may accrue due to alternative cooling arrangements.

TABLE II
Vehicle Simulation Results

Cycle	Description	Si	SiC (x40)	SiC (x30)	Units
UDDS	Fuel consumption	3.683	3.698	3.655	L/100km
		0	0.41	-0.76	%
	Motor & inverter losses	784	807	755	Wh
Urban Artémis	Fuel consumption	4.32	4.29	4.24	L/100km
		0	-0.69	-1.85	%
	Motor & inverter losses	635	626	594	Wh
Road Artémis	Fuel consumption	4.15	4.165	4.135	L/100km
		0	0.36	-0.36	%
	Motor & inverter losses	745	782	731	Wh
Motorway Artémis	Fuel consumption	5.82	5.83	5.815	L/100km
		0	0.17	-0.09	%
	Motor & inverter losses	925	954	903	Wh

Acknowledgment

The authors gratefully acknowledge the support from Cree, Inc. in conducting this work and making prototype SiC components available for the study, as well as the Wisconsin Electric Machines and Power Electronics Consortium (WEMPEC) for their support.

References

[1] D. Aggeler, J. Biela and J. W. Kolar, "A compact, high voltage 25 kW, 50 kHz DC-DC converter based on SiC JFETs," in *Proc. IEEE Applied Power Electronics Conference and Exposition*, Austin, TX, 2008, pp. 801-807.

[2] H. Sheng, Z. Chen, F. Wang and A. Millner, "Investigation of 1.2 kV SiC MOSFET for High Frequency High Power Applications," in *Proc. IEEE Applied Power Electronics Conference and Exposition*, Palm Springs, CA, 2010, pp. 1572-1577.

[3] R. Kelley, M. S. Mazzola and V. Bondarenko, "A scalable SiC device for DC/DC converters in future hybrid electric vehicles," in *Proc. IEEE Applied Power Electronics Conference and Exposition*, Dallas, TX, 2006, pp. 460-463.

[4] H. Zhang, L. M. Tolbert and B. Ozpineci, "Impact of SiC devices on hybrid electric and plug-in hybrid electric vehicles," in *Proc. IEEE Industry Applications Society Annual Meeting 2008*, Edmonton, AB, Canada, pp. 1-5.

[5] E. Vinot, J. Scordia, R. Trigui, B. Jeanneret and F. Badin, "Model simulation, validation and case study of the 2004 THS of Toyota Prius," *International Journal of Vehicle Systems Modelling and Testing*, vol. 3, no. 3, pp. 139-167, 2008.

[6] R. H. Staunton, C. W. Ayers, L. D. Marlino, J. N. Chiasson and T. A. Burress, "Evaluation of 2004 Toyota Prius Hybrid Electric Drive System," Oak Ridge National Laboratory, Oak Ridge, TN, Tech. Rep. ORNL/TM-2006/423, 2006.

[7] JMAG 10 User Manual, 2010, JSOL Corporation.

[8] T. A. Burress, C. L. Coomer, S. L. Campbell, L. E. Seiber, L. D. Marlino, R. H. Staunton and J. P. Cunningham, "Evaluation of the 2007 Toyota Camry Hybrid Synergy Drive System," Oak Ridge National Laboratory, Oak Ridge, TN, Tech. Rep. ORNL/TM-2007/190, 2008.

[9] J. S. Hsu, C. W. Ayers and C. L. Coomer, "Report on Toyota/Prius Motor Design and Manufacturing Assessment," Oak Ridge National Laboratory, Oak Ridge, TN, Tech. Rep. ORNL/TM-2004/137, 2004.

[10] J. K. Tangudu, T. M. Jahns, A. EL-Refaie and Z. Q. Zhu, "Lumped parameter magnetic circuit model for fractional-slot concentrated-winding interior permanent magnet machines," in *Proc. IEEE Energy Conversion Congress and Exposition*, San Jose, CA, 2009, pp. 2423-2430.

[11] MATLAB R2008b User Manual, 2008, The Mathworks.

[12] A. Kawahashi, "A new-generation hybrid electric vehicle and its supporting power semiconductor devices," in *Proc. 16th International Symposium on Power Semiconductor Devices & IC's*, Kitakyushu, Japan, 2004, pp. 23-29.

[13] D. Finn, G. Walker and P. Sernia, "Method of Extracting Switching Loss from a High Efficiency MOSFET Based Half Bridge Converter," in *Proc. Australasian Universities Power Engineering Conference*, 2003, pp. 1-6.

[14] T. Bohn, private communication, February 2010.